



A LETTERS JOURNAL EXPLORING
THE FRONTIERS OF PHYSICS

OFFPRINT

**Anomalous diffusion of wall-bounded
non-colloidal suspensions in a steady shear flow**

KYONGMIN YEO and MARTIN R. MAXEY

EPL, **92** (2010) 24008

Please visit the new website
www.epljournal.org

TARGET YOUR RESEARCH WITH EPL



Sign up to receive the free EPL table of contents alert.

www.epljournal.org/alerts

Anomalous diffusion of wall-bounded non-colloidal suspensions in a steady shear flow

KYONGMIN YEO^(a) and MARTIN R. MAXEY

Division of Applied Mathematics, Brown University - Providence, RI 02912 USA

received 15 July 2010; accepted in final form 11 October 2010

published online 16 November 2010

PACS 47.57.E- – Suspensions

PACS 82.70.-y – Disperse systems; complex fluids

PACS 83.80.Hj – Suspensions, dispersions, pastes, slurries, colloids

Abstract – We investigate the shear-induced diffusion of concentrated non-colloidal suspensions in a Couette flow. The channel is divided into four zones based on the suspension microstructure and variances of the wall-normal and spanwise displacements for the particles in each zone. Due to the strong spatial coherency induced by the density fluctuations, the suspended particles exhibit anomalous diffusion. The diffusion in the wall-normal direction changes from superdiffusion for the particles next to the wall to subdiffusion for the particles near the core of the channel. It seems that the intermittent jumps and particle entrapment in particle layers are responsible for the anomalous diffusion near the wall, while the subdiffusion in the core is related to the overall confinement by the channel walls.

Copyright © EPLA, 2010

Study of the shear-induced diffusion process in non-colloidal suspensions is essential in understanding the dynamics of suspension flows [1–7]. The interaction between three or more particles in Stokes flow is chaotic [8] and, thus, even small non-hydrodynamic effects, which come from, for example, surface roughness or short-range interparticle forces, make the system unpredictable and irreversible [4,9]. As a result, non-colloidal particles in sheared suspensions, where the dynamics is determined mainly by hydrodynamic interactions, exhibit a diffusive behavior similar to colloidal suspensions, where Brownian motion is the driving mechanism [10–12]. Due to a substantial number of studies over the past decade (see [7,13] for review), now our knowledge on the shear-induced diffusion process of concentrated non-colloidal suspensions in an open domain, *i.e.* far from a solid boundary, is much more advanced. However, much less is known about the diffusion process in wall-bounded suspensions.

Most studies of the diffusion processes in confined suspensions have been focused on hard-sphere fluids or colloidal suspensions in thermodynamic equilibrium, *i.e.* in the absence of flow. Mittal *et al.* [14] calculated the position-dependent diffusivity of confined hard-sphere fluids using discontinuous molecular-dynamics

simulations. Michailidou *et al.* [15] have studied the short-time self-diffusion of colloidal suspensions near the wall from both experimental and numerical results. Nugent *et al.* [16] and Sarangapani and Zhu [17] studied the diffusion of colloidal suspensions bounded by two parallel walls for a wide range of the gap width between two walls to investigate the dynamic lengthscale of structural reorganization. Eral *et al.* [18] investigated the effects of smooth and rough walls on the diffusion of concentrated colloidal suspensions. They showed that even in the center of the channel, the particles exhibit subdiffusive behavior. In flowing suspensions, Zurita-Gotor *et al.* [19] estimated the local self-diffusivity in the dilute limit from binary particle interactions. Asmolov [20] has computed the diffusion of non-colloidal particles in dilute wall-bounded suspensions (volume fraction $\phi \leq 0.02$) under a steady shear using a constant dipole model. Still, there is only a limited number of studies on the shear-induced diffusion in wall-bounded concentrated suspensions.

In this letter, we study the confinement effects on suspension dynamics focusing on the crossflow diffusion of the particles as a function of the distance from the wall on the intermediate timescale $t^* \sim O(100)$, in which t^* is the time normalized by the shear rate $\dot{\gamma}$, $t^* = \dot{\gamma}t$. The main results are presented for concentrated suspensions in a wall-bounded Couette flow, where the bulk volume fraction is $\phi = 0.40$. The channel is divided into four zones,

^(a)E-mail: kyeo@dam.brown.edu

considering the suspension microstructure [21], and the behavior of particles in each zone is investigated. Particularly, we are interested in the variance of particle displacement, which is a measure of the spreading of the suspended particles relative to the mean position. It is found that the variance of the wall-normal displacement shows anomalous diffusive behavior, $\sigma_y^2 \sim t^\nu$, in which $\nu \neq 1$. Depending on the initial location, particles exhibit super- ($\nu > 1$) or subdiffusion ($\nu < 1$) in the velocity gradient (wall-normal) direction. Anomalous diffusion has been observed in transport processes in porous media [22] or passive tracer dispersion in flows with coherent structures [23–25]. In this paper, we study anomalous diffusion induced not by a coherent structure in flow but by complex multi-body hydrodynamic interactions. The anomalous diffusion near the wall is linked to strong intermittency of particle motion. Unexpectedly, even particles in the core of the channel show a subdiffusive behavior, which may be related with the restriction on the available lengthscale by the confinement. The diffusive behaviors of particles in the core of the channel for four different volume fractions ($\phi = 0.25, 0.30, 0.35$, and 0.40) are compared.

We use the force-coupling method (FCM) to compute the hydrodynamic interactions. In FCM, long-range multibody interactions are calculated by solving the Stokes equations with regularized, low-order multipoles and viscous lubrication interactions are computed simultaneously by inverting a resistance matrix constructed by the sum of pair interactions [26]. The Stokes equations are solved by using a Fourier spectral method in the velocity (x) and the vorticity (z) directions and the spectral element method in the velocity gradient direction (y). The computational domain size is $H_x \times H_y \times H_z = 30a \times 30a \times 20a$, in which a is the particle radius and x , y , and z denote the velocity (streamwise), velocity gradient (wall-normal), and vorticity (spanwise) directions, respectively. The periodic boundary conditions are used in the horizontal ($x-z$) directions. The no-slip boundary condition is used on the wall. Unless otherwise stated, all results are obtained at the volume fraction $\phi = 0.4$ with 1718 neutrally buoyant spheres. A smooth repulsive potential is applied for particle pairs whose center-to-center distance is smaller than $2.01a$ [21]. The magnitude of the contact force is determined to keep the minimum separation distance between particle surfaces $a\epsilon_{min} \simeq 0.002$. The initial particle configuration is obtained by a molecular-dynamics procedure [27]. Simulations are performed until the system reaches a stationary state. All of the results are obtained after the suspension reaches the stationary state.

Figure 1(a) shows the area fraction ϕ_A as a function of the distance from the wall. $\phi_A(y)$ is defined by $\phi_A(y) = \iint \chi(\mathbf{x}) dx dz / (H_x \times H_z)$, where $\chi(\mathbf{x})$ is a particle-phase indicator function. A significant fluctuation of ϕ_A is observed near the wall. Due to the strong particle-wall lubrication interaction, a well structured particle layer develops near the wall (Zone I). Above the particle layer,

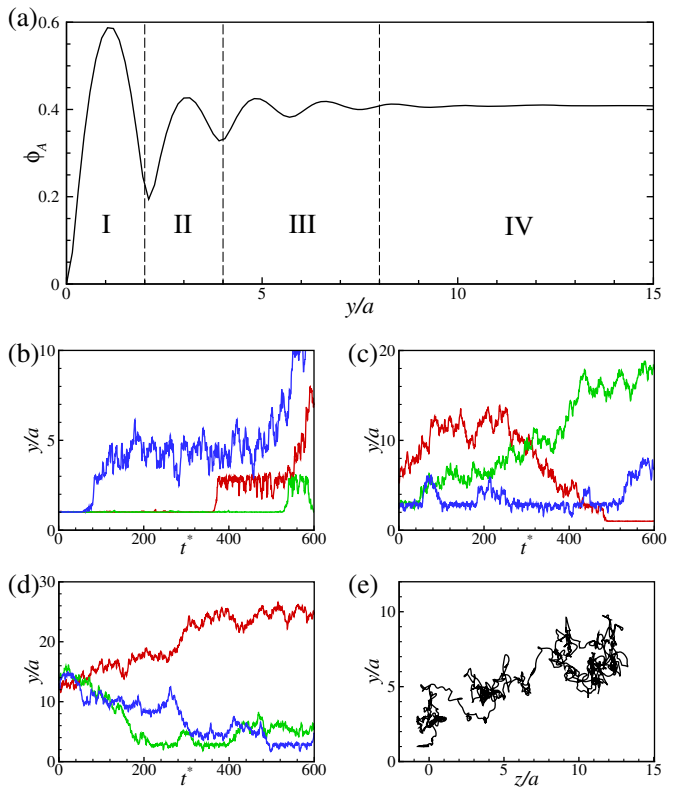


Fig. 1: (Color online) (a) Area fraction profile for the bulk volume fraction $\phi = 0.4$. Considering the symmetry, ϕ_A is shown only for the lower half of the channel. The wall-normal displacements as a function of time are shown for particles which are initially in (b) Zone I, (c) Zone II+III, and (d) Zone IV. (e) shows a representative trajectory in the y - z plane for a particle whose initial location is in Zone I.

there is a region in which the behavior of the suspension flow is still strongly affected by the wall (Zone II). In the core region (Zone IV), the rheology of suspension flow behaves similarly to a homogeneous shear flow. There is a buffer region (Zone III) between the discrete (Zone I+II) and the continuous (Zone IV) regimes. Detailed analysis of the rheology and suspension microstructure in each zone is given in Yeo and Maxey [21].

Figures 1(b)–(d) illustrate the trajectories of particles whose initial locations are in (b) Zone I, (c) Zone II+III, and (d) Zone IV. Most particles in Zone I stay in the first particle layer for a long period of time $t^* \simeq O(100)$ before moving to Zone II. In Zone II, the particles are again trapped in the second particle layer ($y/a \simeq 3$). The existence of another particle layer is observed around $y/a \simeq 5$, in which the wall-normal displacement is largely restricted to $4 < y/a < 6$ for a long period of time. In fig. 1(c), it is shown that some particles in Zone II move toward the core of the channel while some particles are trapped in the second or third particle layers exhibiting oscillatory motions around $y/a \simeq 3$ or 5 . In contrast, the particles in Zone IV exhibit more standard diffusive behavior (fig. 1(d)). However, some of the particles in Zone

IV migrate towards the wall relatively quickly ($t^* \simeq 200$) and they are trapped in the particle layers. Figure 1(e) shows a representative trajectory of a particle initially located in Zone I plotted in the y - z plane. The wall-normal displacement of the particles in the particle layers ($y/a < 7$) is strongly suppressed by cages formed by the surrounding particles, while the particles are more mobile in the horizontal direction (z). A similar behavior has been observed for confined hard-sphere fluids in equilibrium, where the diffusivity in the horizontal direction is larger than that in the wall-normal direction [14]. Near the wall, the travel time of a particle between each particle layers is much shorter than the residence time inside of the particle layers. The particle trajectories suggest that there is a strong spatial coherence induced by the wall in concentrated suspensions. Moving from the first particle layer (Zone I) to the second (Zone II) and the third particle layers (Zone III), the residence time of a particle in each particle layer decreases and, at the same time, the wall-normal fluctuation around the center of a particle layer becomes stronger.

The variance of each component of the particle displacement is defined as $\sigma_i^2(t) = \langle \tilde{Y}_i^2(t) \rangle - \langle \tilde{Y}_i(t) \rangle^2$, in which $\mathbf{Y}(t)$ is the location of a particle at time t and $\tilde{\mathbf{Y}}(t) = \mathbf{Y}(t) - \mathbf{Y}(0)$. Figure 2(a) shows the normalized variance ($\sigma^{*2} = \sigma^2/a^2$) for the particles in Zone I at $t^* = 0$. σ^2 in both y and z directions show a ballistic behavior $\sim t^2$ for short time intervals while the particle velocity remains strongly correlated. For $t^* \sim O(100)$, both σ_y^2 and σ_z^2 grow faster than $\sim t$, indicating superdiffusion. In the inset of fig. 2(a), it is clearly seen that $\sigma_y^2 \sim t^{1.69}$ and $\sigma_z^2 \sim t^{1.17}$. In homogeneous suspensions, the variances are highly anisotropic and $\sigma_y^2(t)/\sigma_z^2(t) > 1$ [4]. However, in Zone I, σ_y^2 is much smaller than σ_z^2 .

Figure 2(b) shows the probability density functions (PDF) for the normalized wall-normal displacement. The PDFs are computed for the particles in Zone I at $t^* = 0$. Here, the normalized wall-normal displacement is defined as $y^* = (\tilde{Y}_2(t) - \langle \tilde{Y}_2(t) \rangle) / \sigma_y(t)$. The normalized PDFs show a remarkable self-similarity. The positive tails of the PDFs almost collapse onto one curve after the superdiffusion is observed ($t^* > 200$). The tail of the PDF shows an exponential decay $\sim \exp(-\alpha y^*)$ with $\alpha = 0.8$. As a measure of the intermittency, we computed the flatness factor, which is the fourth moment of the normalized PDF. The flatness factor of the PDF is about 18, compared to 3 of a Gaussian distribution, indicating that there is a large fraction of the particles, which travel in a much faster rate compared to the mean spreading rate. The intermittent events, jumps to Zone II and III shown in figs. 1(b), (c), seem to be responsible for the slow decay of the PDF.

Figure 3 shows the changes of the PDF of the wall-normal particle velocity (V_2) in time for the particles initially located in Zone I. The particle velocity is normalized as $V_2^* = (V_2(t) - \langle V_2(t) \rangle) / \sigma_V(t)$, in which σ_V is the standard deviation of V_2 . The third moments of the

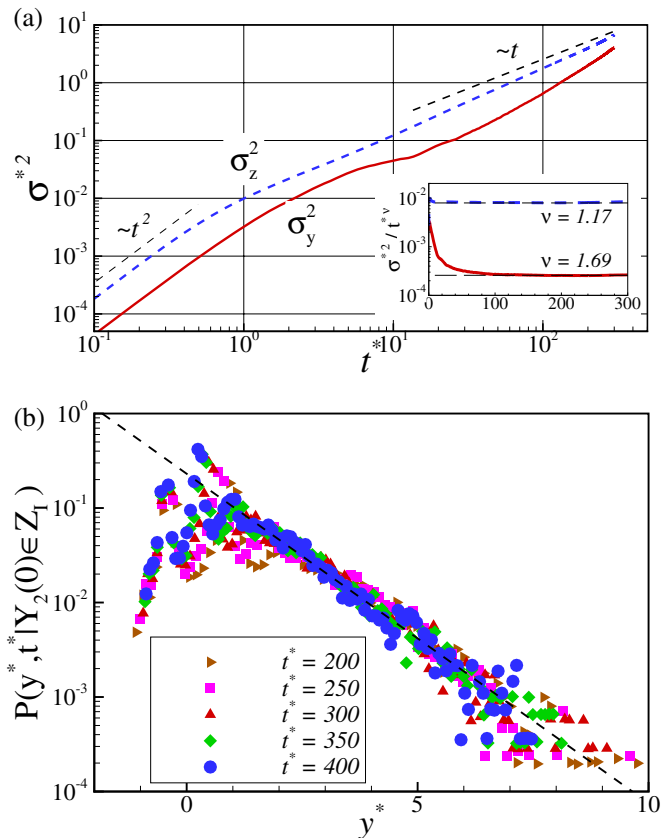


Fig. 2: (Color online) (a) Variances of the wall-normal and spanwise displacements of the particles in Zone I at $t^* = 0$. The inset shows the variances divided by t^ν . (b) The probability density functions (PDF) of the standardized wall-normal displacements at different time instances. The dashed line is $\sim \exp(-0.8y^*)$.

normalized PDFs in fig. 3(a) are about 0.1, suggesting that the wall-normal velocity PDFs $P(V_2^*)$ are nearly symmetric. Similar to the wall-normal displacement PDF, $P(V_2^*)$ has a much wider tail compared to the Gaussian distribution. The flatness factor of $P(V_2^*)$ is a decreasing function of time. The flatness factors are 18, 13, and 10 at $t^* = 200, 300, \text{ and } 400$, respectively. This decrease of the flatness factor in time is related with the reduced frequency of the intermittent events, as the particles migrate into Zone III and IV.

To investigate the changes of $P(V_2^*)$ in time in more detail, the positive tail of $P(V_2^*)$ is shown in a log-log plot in fig. 3(b). Interestingly, $P(V_2^*)$ consists of three distinctive ranges. In the central range of small V^* , the velocity PDF shows an algebraic decay $\sim V_2^{*\beta}$ with $\beta \simeq -2$. The V^{*-2} behavior in this core seems to be due to the particles remaining in Zone I. For comparison, $P(V_2^*)$ at $t^* = 10$, when most of the particles are still in Zone I, is drawn in the same plot. It is shown that $P(V_2^*)$ at $t^* = 10$ is well approximated by V^{*-2} . Around $V_2^* \simeq 0.3 \sim 0.4$, the exponent β changes from -2 in the core to $-1/2$ in an intermediate range. The crossover point gradually moves towards the origin as the particles leave Zone I and migrate

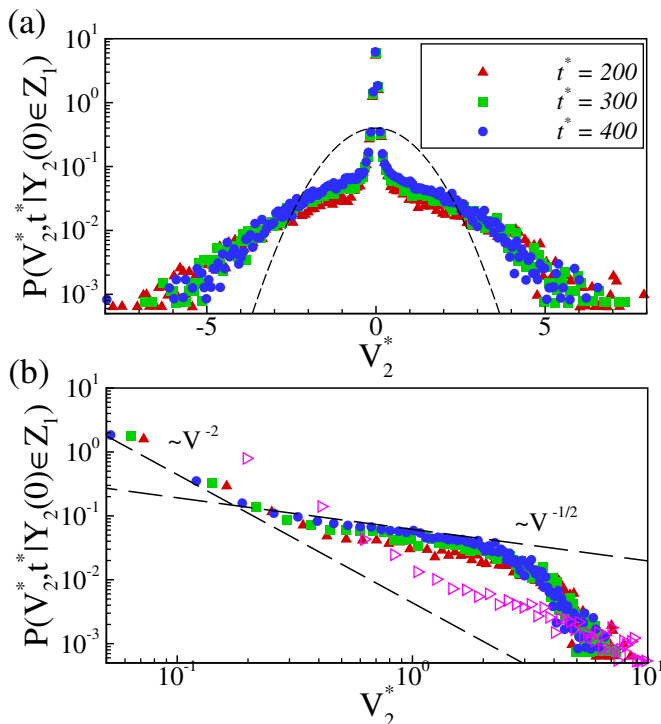


Fig. 3: (Color online) (a, b) PDFs of the wall-normal velocity V_2 of the particles initially located in Zone I. The velocity PDFs are shown for $t^* = 200, 300$, and 400 . The dashed line in (a) is the Gaussian distribution. In (b), \triangleright is the velocity PDF for $t^* = 10$.

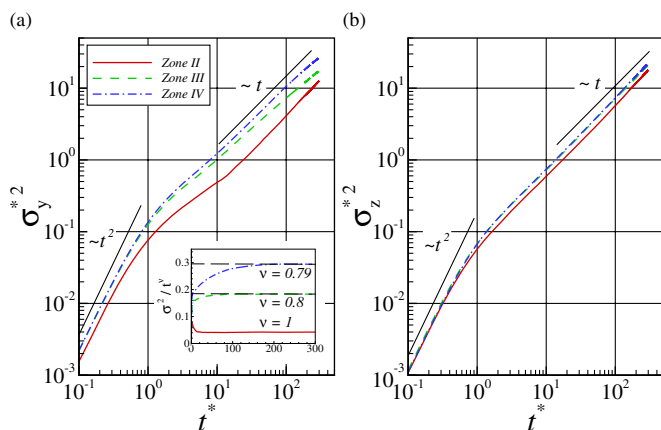


Fig. 4: (Color online) Variances of the (a) wall-normal and (b) spanwise displacements of particles in Zones II–IV.

to the channel center. A mechanism responsible for the slow decay $\sim V^{*-1/2}$ is not clear. The behavior seems to be related with the particles in Zone II or III. However, the $V^{*-1/2}$ behavior is somewhat surprising, because the velocity PDF for the particles in other Zones, even that calculated in Zone II, is essentially Gaussian. For large V_2^* , $P(V_2^*)$ shows an exponential decay.

σ_y^2 for Zones II–IV are shown in fig. 4(a). As the diffusive behavior changes from superdiffusion in Zone I to

subdiffusion in Zones III, Zone II shows normal diffusion ($\sigma^2 \sim t$) with $D_y^* = 2.1 \times 10^{-2}$, in which D^* is the diffusivity normalized by $\dot{\gamma}a^2$. In fig. 1(a), it is shown that ϕ_A reaches a plateau in Zone IV, implying that the suspension may behave similarly to a homogeneous suspension. Indeed, rheology and suspension microstructure in Zone IV are comparable to those in homogeneous suspensions [21]. Therefore, it is natural to assume that σ^2 would show normal diffusion as in homogeneous suspensions. Unexpectedly, the particles in Zone IV exhibit subdiffusion for $t^* > 150$. The inset shows the variances divided by t^ν . It is shown that $\sigma_y^2 \sim t^{0.8}$ for the particles in Zones III and $\sigma_y^2 \sim t^{0.79}$ for Zone IV.

Figure 4(b) shows σ_z^2 for Zones II–IV. Unlike σ_y^2 , normal diffusion is observed in the vorticity direction. In the wall-normal displacement, the variance for Zone IV is significantly larger than that for Zone III; $\sigma_y^2 = 17.5$ and 26.6 at $t^* = 300$ for Zone III and IV, respectively. However, σ_z^2 for Zone III and IV are almost the same; 21.4 and 22.3 for Zone III and IV, respectively, at $t^* = 300$. In fig. 1(e), it is observed the wall-normal movement is strongly suppressed near the wall while the spanwise displacement is less restricted. As a result, σ_z is larger than σ_y for Zones I–III. In Zone IV, σ_y becomes larger than σ_z similar to the results in homogeneous suspensions. The diffusivities in the vorticity direction computed from σ_z^2 are $D_z^* = 3.1 \times 10^{-2}$, 3.6×10^{-2} , and 3.7×10^{-2} for Zone II, III, and IV, respectively. D_z^* in Zone III and IV are similar to that in homogeneous shear flow [26].

The changes of area fraction profiles in time for different initial groups of particles are shown in fig. 5. As the outward flux from Zone I should be equal to the inward flux from Zone II to Zone I, the particles in Zone II have much higher probability of migrating towards the core (Zone III + IV). In fig. 5(a), it is shown that only a small fraction of particles move into Zone I while most of them migrate towards the outer region, which may explain the apparent normal diffusion in Zone II (fig. 4(a)). On the other hand, for the particles in Zone III, a large fraction of particles move to Zone I + II, in which they are trapped in particle layers (fig. 5(b)). For $y/a > 6$, the spreading of ϕ_A to Zone IV is almost Gaussian. However, for $y/a < 6$, ϕ_A shows a complex behavior as particles migrate into Zone II and subsequently into Zone I. ϕ_A in Zone I is an increasing function of t^* , while ϕ_A in the second particle layer ($y/a \simeq 3$) stays almost constant for $t^* = 100$ – 400 . Subdiffusion may occur if there are stagnation or recirculating regions in the fluid flow, in which particles are arrested [25]. The subdiffusion in Zone III can be understood in the same context. Some particles in Zone III quickly move to the near wall region and they are trapped in the particle layers hovering around the same wall-normal position for a long time, while others migrate to the channel core. However, for Zone IV, only a small fraction of the particles reach Zones I and II and most of the particles remain in Zones III and IV in the time interval

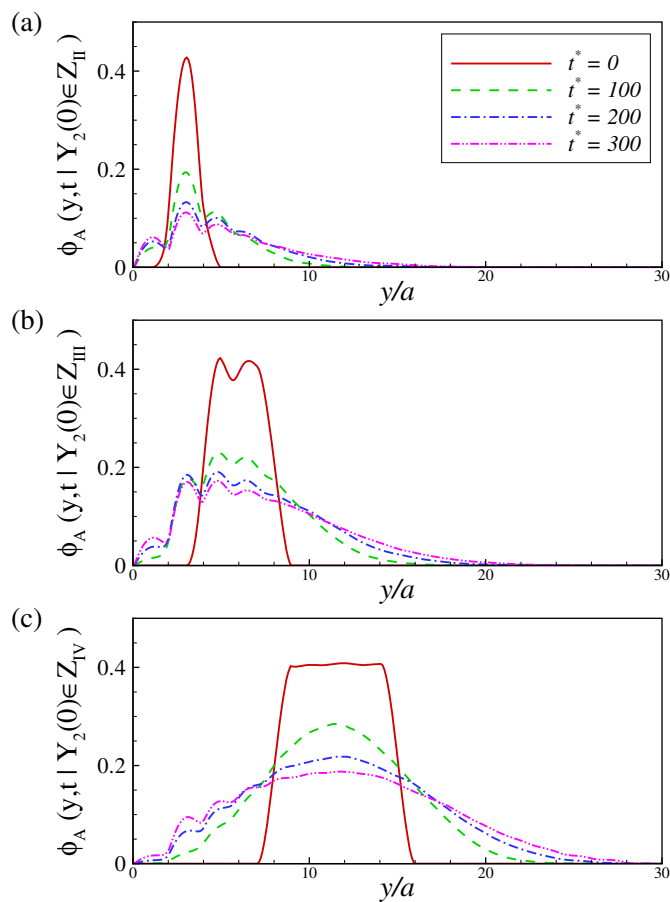


Fig. 5: (Color online) The area fraction profiles at different time instances for the particles whose initial locations are in (a) Zone II, (b) Zone III, and (c) Zone IV.

considered (fig. 5(c)). The subdiffusion in Zone IV cannot be explained solely by the particle entrapment in the near-wall region.

To investigate the diffusive behavior of the particles in the core of the channel more clearly, σ_y^2 is computed for the particles only near the center of the channel, $12 \leq y/a \leq 18$, for $0.25 \leq \phi \leq 0.40$ (fig. 6(a)). At $t^* = 200$, $\sigma_y^* = 2.87, 3.58, 4.18,$ and 4.54 for $\phi = 0.25, 0.30, 0.35,$ and 0.40 , respectively, indicating that most of the particles have not reached the near-wall region (Zone I+II) yet.

The variances in the wall-normal direction divided by t^* are shown in fig. 6(b). For $\phi = 0.25$, normal diffusion is observed for $t^* > 50$ with $D_y^* = 2.1 \times 10^{-2}$. However, for $\phi \geq 0.30$, subdiffusive behaviors are observed for $t^* > 100$. Considering that σ_y^* at $t^* = 100$ are $2.59, 3.02,$ and 3.32 for $\phi = 0.30, 0.35,$ and 0.40 , respectively, the origin of the subdiffusivity is not the particle entrapment as in the case of Zone III. For $\phi = 0.25$, it is interesting to observe that the linear region ($\sim t$) is developed for $t^* > 50$, while such a linear behavior has been observed at smaller t^* in homogeneous suspensions ($t^* > 20$) [4].

One possible explanation of this subdiffusive behavior is the restriction on the lengthscale of suspension

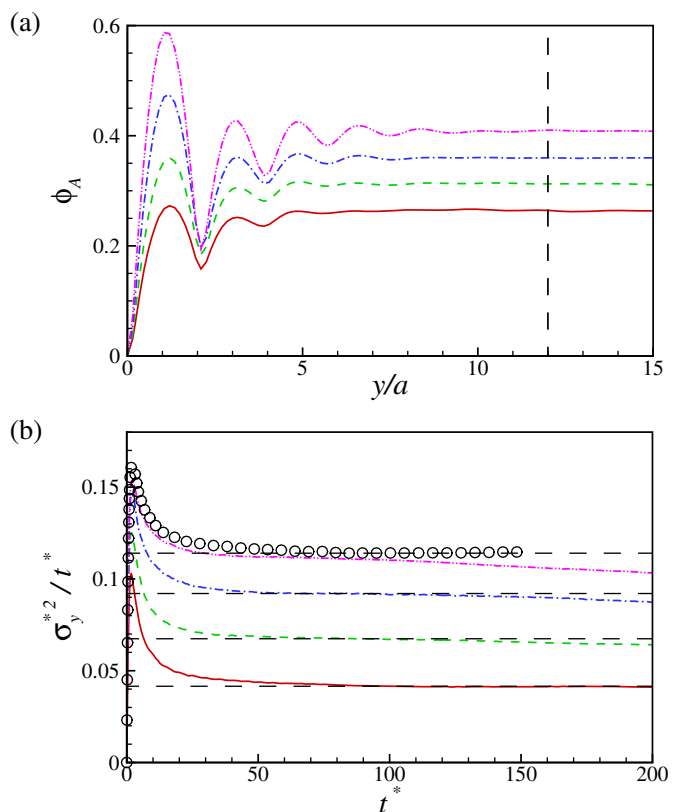


Fig. 6: (Color online) The area fraction profiles (a) and variances of the wall-normal displacement (b) for $\phi = 0.25$ (—), 0.3 (---), 0.35 (-·-·-), and 0.40 (-·-·-), $H_y/a = 30$. In (b), the circles are for $\phi = 0.40$ and $H_y/a = 40$.

flows by the size of confinement. In previous studies of confinement effects on the dynamics of equilibrium colloidal suspensions, it has been shown that, as the lengthscale of structural reorganization is limited by H_y/a , the mobility of particles and relaxation processes are significantly slowed [16–18]. In sheared suspensions, the dynamics is closely related to the formation of hydroclusters, which have a long correlation length [28]. However, in a confined suspensions, the lengthscale available for the formation of hydroclusters is limited by the confinement size and the emergence of a wall-induced microstructure, namely, a particle layer. For example, for $\phi = 0.40$ and $H_y/a = 30$, the suspension field is uniform only in $10 < y/a < 20$, indicating that the available lengthscale for a shear-induced suspension structure to develop is only $L \sim 10a$. This restriction on lengthscale may disable some of large-scale dynamic modes. The disturbance of these large-scale collective motions leads to the subdiffusion on the intermediate timescale $t^* \sim O(100)$, over which normal diffusion has been observed in homogeneous suspensions.

To support the argument, σ_y^2 for $\phi = 0.40$ and $H_y/a = 40$ is shown in fig. 6(b), where σ_y^2 is computed from the particles in the core of the channel $17 \leq y/a \leq 23$. Normal diffusion is observed from $t^* > 50$ with $D_y^* = 5.7 \times 10^{-2}$,

which is comparable to the result in homogeneous suspensions [29], suggesting that the $H_y/a = 40$ channel is large enough to accommodate a large-scale suspension structure. This observation is consistent with the experiments of [30], where they found that the suspension rheology is independent of H_y , when $H_y/a > 40$. Comparing $\phi = 0.25$ to 0.30 , the diffusive behavior changes from normal diffusion at $\phi = 0.25$ to subdiffusion at $\phi = 0.30$, though the available lengthscales estimated from the ϕ_A profiles are similar, suggesting that the lengthscale of the hydroclusters increases with the volume fraction. However, to confirm the changes of the lengthscale with ϕ , extensive studies for a wide range of ϕ_A and H_y/a are still required.

We have shown that concentrated non-colloidal suspensions in a wall-bounded Couette flow exhibit anomalous diffusion on the intermediate timescale, on which normal diffusion is observed for homogeneous suspensions. Based on our previous study [21], the channel is divided into four zones and the behavior of particles in each zone is investigated. For the diffusion perpendicular to the wall, particles exhibit anomalous diffusion due to a strong spatial coherency induced by the wall effects. Particularly, the particles in a well-structured particle layer located next to the wall (Zone I) show superdiffusive behavior. The probability density functions both for the displacement and the wall-normal velocity show wider tails compared to the Gaussian distribution, indicating the stochastic processes involved in the motion of the particles are highly intermittent. Subdiffusion is observed for the particles in Zone III and IV. As a buffer zone between superdiffusion in Zone I and subdiffusion in Zone III, normal diffusion is observed in Zone II. The subdiffusion in Zone III is related with the trapping of the particles in the particles layers near the wall, Zone I + II. In confined suspensions, the available lengthscale for the suspension dynamics is restricted by the size of the confinement, which will disable some of the large-scale dynamic modes [18]. The subdiffusion in Zone IV seems to be related with a disturbance in large-scale collective motions, such as the formation of hydroclusters, by the size of the confinement. As the volume fraction increases from $\phi = 0.25$ to 0.40 , the diffusive behavior of the particles in the channel center changes from normal to subdiffusion, implying the largest lengthscale related with suspension dynamics increases with the volume fraction. It is worthwhile to note that, while most modeling approaches to suspension flows are based on the results in homogeneous suspensions, the present study indicates that the models may fail to predict the diffusive behavior not only near the wall (Zone I + II) but also in the core (Zone IV).

REFERENCES

- [1] LEIGHTON D. and ACRIVOS A., *Chem. Eng. Sci.*, **41** (1986) 1377.
- [2] NOTT P. R. and BRADY J. F., *J. Fluid Mech.*, **275** (1994) 157.
- [3] ACRIVOS A., *J. Rheol.*, **39** (1995) 813.
- [4] DRAZER G., KOPLIK J., KHUSID B. and ACRIVOS A., *J. Fluid Mech.*, **460** (2002) 307.
- [5] SEMWOGERERE D., MORRIS J. F. and WEEKS E. R., *J. Fluid Mech.*, **581** (2007) 437.
- [6] FALL A., BERTRAND F., OVARLEZ G. and BONN D., *Phys. Rev. Lett.*, **103** (2009) 178301.
- [7] MORRIS J. F., *Rheol. Acta*, **48** (2009) 909.
- [8] JÁNOSI I. M., TÉL T., WOLF D. E. and GALLAS J. A. C., *Phys. Rev. E*, **56** (1997) 2858.
- [9] PINE D. J., GOLLUB J. P., BRADY J. F. and LESHANSKY A. M., *Nature*, **438** (2005) 997.
- [10] ECKSTEIN E. C., BAILEY D. G. and SHAPIRO A. H., *J. Fluid Mech.*, **79** (1977) 191.
- [11] LEIGHTON D. and ACRIVOS A., *J. Fluid Mech.*, **181** (1987) 415.
- [12] BREEDVELD V., VAN DEN ENDE D., JOMGSCHAAP D. and MELLEMA R., *J. Chem. Phys.*, **114** (2001) 5923.
- [13] STICKEL J. J. and POWELL R. L., *Annu. Rev. Fluid Mech.*, **37** (2005) 129.
- [14] MITTAL J., TRUSKETT T. M., ERRINGTON J. R. and HUMMER G., *Phys. Rev. Lett.*, **100** (2008) 145901.
- [15] MICHAÏLIDOU V. N., PETEKIDIS G., SWAN J. W. and BRADY J. F., *Phys. Rev. Lett.*, **102** (2009) 068302.
- [16] NUGENT C. R., EDMOND K. V., PATEL H. N. and WEEKS E. R., *Phys. Rev. Lett.*, **99** (2007) 025702.
- [17] SARANGAPANI P. S. and ZHU Y., *Phys. Rev. E*, **77** (2008) 010501(R).
- [18] ERAL H. B., VAN DEN ENDE D., MUGELE F. and DUTS M. H. G., *Phys. Rev. E*, **80** (2009) 061403.
- [19] ZURITA-GOTOR M., BLAWZDZIEWICZ J. and WAJNRYB E., *J. Fluid Mech.*, **592** (2007) 447.
- [20] ASMOLOV E. S., *Phys. Rev. E*, **77** (2008) 066312.
- [21] YEO K. and MAXEY M. R., *J. Fluid Mech.*, **649** (2010) 205.
- [22] DRAZER G. and ZANETTE D. H., *Phys. Rev. E*, **60** (1999) 5858.
- [23] OTTINO J. M., *Annu. Rev. Fluid Mech.*, **22** (1990) 207.
- [24] SOLOMON T. H., WEEKS E. R. and SWINNEY H. L., *Phys. Rev. Lett.*, **71** (1993) 3975.
- [25] YOUNG W. R., *J. Fluid Mech.*, **193** (1988) 129.
- [26] YEO K. and MAXEY M. R., *J. Comput. Phys.*, **229** (2010) 2401.
- [27] YEO K. and MAXEY M. R., *Phys. Rev. E*, **81** (2010) 051502.
- [28] MELROSE J. R. and BALL R. C., *J. Rheol.*, **48** (2004) 961.
- [29] SIEROU A. and BRADY J. F., *J. Fluid Mech.*, **506** (2004) 285.
- [30] ZARRAGA I. E., HILL D. A. and LEIGHTON D. T., *J. Rheol.*, **44** (2000) 185.